

# Experimental Assessment of Simultaneous In-Situ Heliostats Calibration Methodology HelioControl at Themis Facility

Gregor Bern<sup>1,a)</sup>, Moritz Bitterling<sup>1</sup>, Peter Schöttl<sup>1</sup>, Alain Ferriere<sup>2</sup>, Yann Volut<sup>2</sup>,  
Anna Heimsath<sup>1</sup> and Peter Nitz<sup>1</sup>

<sup>1</sup>Fraunhofer Institute for Solar Energy Systems ISE. Heidenhofstr. 2, 79110 Freiburg, Germany.

<sup>2</sup>CNRS/PROMES, 7 rue du four solaire, 66120 Font-Romeu, France

<sup>a)</sup>Corresponding author: gregor.bern@ise.fraunhofer.de

**Abstract.** An imaging method for the parallel in-situ measurement of heliostat aim points during operation in central receiver systems is assessed. In a SFERAII-access campaign, the HelioControl prototype system was integrated into the heliostat control system Hyperviseur at the Themis facility. The method, determining aim points from the cumulative flux distribution at the receiver, uses a signal of periodic movement, modulated by means of the heliostat drives. The functionality was implemented into a group of heliostats and practically assessed. For few heliostats, exemplary parallel aim point measurements at a flux target – using the methodology – show very small differences compared to a reference. Further experiments with multiple overlapping focal spots have been conducted using the small experimental cavity receiver of the system. The highly variable reflectance of the receiver area is challenging for the imaging method evaluating the reflection of the incident flux. A simplified receiver model obtained from experiments with single heliostats, however, allows for a correction and preliminary evaluation. The promising results obtained from measurements with deviations below 0.7 mrad in exemplary evaluations display the potential of the method and motivate for further and comprehensive validation in the context of commercial scale central receiver systems.

## INTRODUCTION

Current central receiver systems use open loop systems to control the heliostat field. Most of these systems rely on calibration algorithms as described by Berenguel et al.<sup>1</sup>. Drift models<sup>2,3</sup> improve the open loop tracking accuracy, but demand for a high number of calibration measurements, reducing the power available for production. Closed loop systems involving cameras<sup>4</sup> or sensors<sup>5</sup> around the receiver or attached to the heliostats (e.g. Harper et al.<sup>6</sup>) have been presented. The only closed loop system in operation involves cameras included into the receiver with a special pinhole design<sup>7</sup>, implemented in the Ashlim power plant. Other closed loop systems have, to our knowledge, not yet been deployed in commercial operation.

An imaging method for the identification and measurement of heliostat aim points among a high number of overlapping flux contributions during operation has been first introduced in 2017<sup>8</sup> and further assessed on a theoretical basis<sup>9</sup>. The measurement system is intended either for the fast calibration of a heliostat fields or for applying a closed loop scheme with a regular correction of the heliostat aim points during normal operation. Earlier publications involved theoretical calculations, assessment of simulated flux distributions and evaluation of laboratory experiments. This work presents practical assessments of the HelioControl methodology that have been performed within the SFERAII access programme in the solar tower test facility Themis, operated by CNRS/PROMES, France, and discusses the promising results obtained.

# METHODOLOGY

## The HelioControl Plug-In

The HelioControl concept allows for the simultaneous identification of the representative true aim points of multiple heliostats during operation by means of image sequence analysis. The low intrusive plug-in concept allows the integration into new or existing heliostat control systems via a simple communication link. A scheme of the method is given in Fig. 1(a): during operation of the plant, the heliostat field control system controls a group of heliostats to perform a small periodic movement around their respective axes, using the heliostats primary or secondary drives. The frequency of movement is different for each heliostat. An exemplary profile of movement is given in Fig. 1(b). A camera observing the receiver captures a sequence of images for further evaluation in the target measurement unit, i.e. the HelioControl-plug-in. The latter extracts the individual representative aim points of the individual heliostats and forwards this information to the field control for comparison with the command position and correction of heliostat tracking parameters. The details of the method are explained in detail in earlier publications<sup>9</sup>. The HelioControl concept has been implemented as a prototypical measurement system capable of performing GPU-supported real time evaluations.

## Integration in Themis Facility

The first step in the project was the modification of the heliostat control infrastructure at Themis to allow for the controlled stimulation of periodical movements of a group of heliostats. The functionality for triggering such movement and controlling its characteristic was integrated in the newly developed field control interface of Themis, Hyperviseur. The movement was defined by an amplitude in heliostat drive increments and a factor defining the maximum speed of movement. Figure 1b shows a sketch of the defined movement: the primary or secondary drive accelerates until its maximum speed has been reached. It proceeds in the direction of movement until an amplitude-threshold has been reached, somewhere below the total amplitude of movement. After deceleration, the movement is repeated in the other direction of rotation. The acceleration, however, could not be defined precisely due to the controller programming architecture. Hence, the frequencies of movement related to different settings were measured afterwards in a first group of experiments. On real time drive controller systems, the full movement could be defined precisely according to Fig. 1b.

The implementation of the periodic movement was integrated into the local heliostat drive controller units of four heliostats. Figure 2 shows a scheme of the heliostat field and orientation at Themis facility. The heliostats marked in red have been equipped with the new functionality.

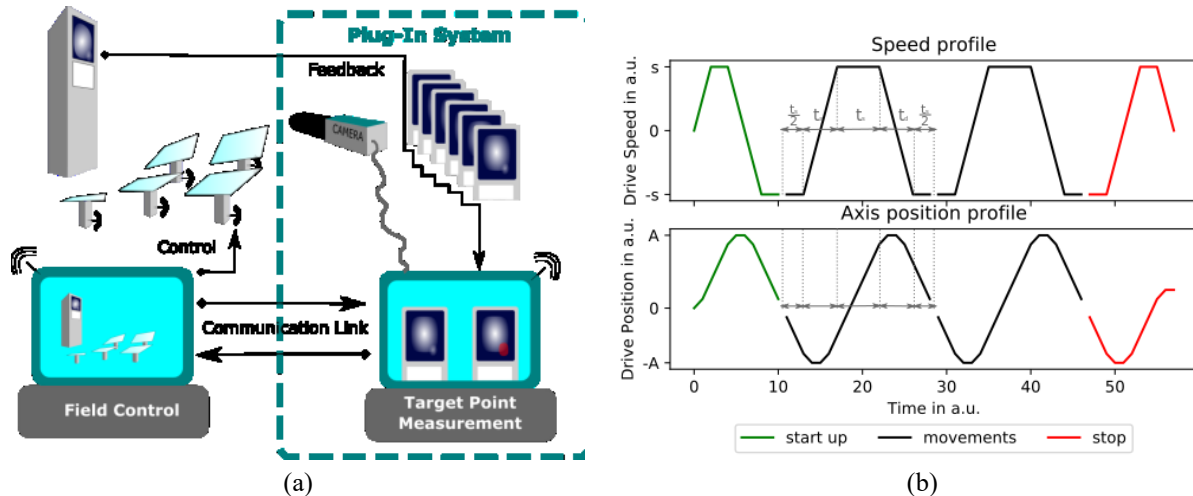


**Figure 1:** (a) Scheme of the HelioControl method<sup>9</sup>: The field control system controls a group of heliostats to perform a small periodic movement. Images of the flux at the receiver are captured, processed and the extracted representative aim point of the individual heliostats is returned to the heliostat field control system. (b) Exemplary speed profile of a heliostat drive to perform a periodic movement. A similar profile was implemented at the Themis facility.

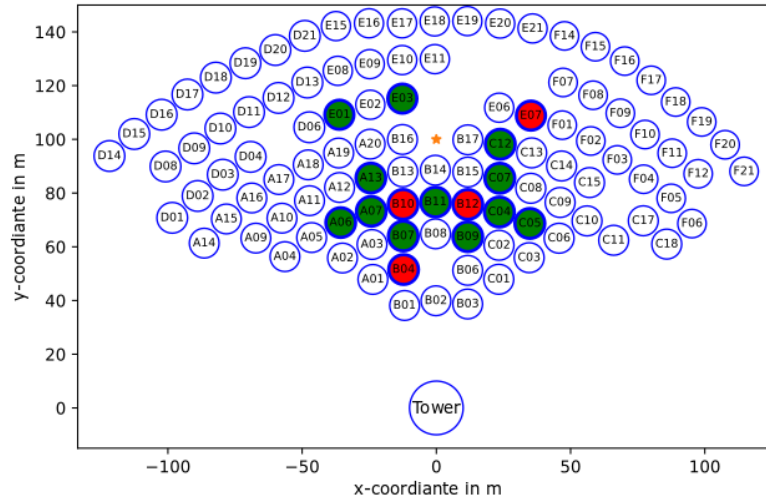


Figure 2: Scheme of the heliostat field at the Themis facility in Targassonne, France, including heliostat IDs. The four heliostats marked in red have been equipped with the capability of performing a periodic movement with defined frequencies. The heliostats marked in green were used in normal tracking mode to add flux during the experiments. The yellow asterisk marks the position of the control room with the camera, observing the targets at the tower.

Besides the ability to control the heliostats to perform the required movement, a communication link has been established between the heliostat field control system Hyperviseur and the HelioControl plug-in prototype system. The communication was implemented based on a simple protocol for the exchange of commands and measurement results through a serial communication interface. Nevertheless, information was exchanged reliably and quick. In the future, common protocols like ModbusTCP will be available as well.

For measuring the frequency of movement in the elevation axis, an inclinometer was installed at two heliostats. Additionally, the frequency was measured visually by observing the movement and taking the time with a clock. 15 different configurations of speed and amplitude have been recorded of which four were chosen for use in the following experiments.

## MEASUREMENTS

Various measurements have been conducted with increasing complexity, of which three will be presented here. The first represents a simplified assessment with two heliostats aiming at a white flux target installed below the receiver. The second and third presented experiments demonstrate the measurement at the small cavity receiver “Mini-Pegase” at the Themis plant.

Experiments with single heliostats on uniform and diffuse targets allow for the identification of reference positions from interrelation with common means (e.g. according to Berenguel et al.<sup>1</sup>). In contrast, the present cavity receiver is very challenging for a methodology analyzing the reflective area in view. The highly variable reflectance with partially specular characteristics of the receiver disturbs the image analysis process. In this work, we show how the application of a simple reflectance model of the receiver, derived from experimental data, facilitates the evaluation of the image data. State-of-the-art external receivers or cavities, however, do not exhibit the same complex characteristics as the experimental setup, thus allowing for a much simpler evaluation. The experiments at Themis represent a “worst case” scenario for this application, thus revealing the potential for much simpler conditions at commercial external or cavity receivers.

The primary result of the image aim point derivation is given in image coordinates, defined by the camera perspective on the surface under inspection. The heliostat control system bases on the locally defined geometry of Themis with all relevant components and heliostat position in 3D coordinates. Image coordinates from the evaluation must be interrelated with this coordinate system to provide meaningful and comparable information. For translating the data collected with the camera from image coordinates into the coordinate system of the Themis plant, a translation matrix has been generated from image points and corresponding coordinates of the objects in view. In this simplified approach, the coordinates are projected into the image plane, disregarding depth, namely the

Y-direction (compare Fig. 2). In the future, a 3D model can be implemented into the HelioControl-plugin-in to allow for the projection of the identified aim point position to precise local world coordinates, independent of receiver geometry complexity.

The definition of terms used in the following is given in Fig. 3. The *reference position* denotes the expected aim point at the target with *uncertainty*. It is marked in red in Fig. 3a. The measured aim point is marked as a green cross at the center of mass of the identified focal spot. The *deviation* describes the distance between reference position and measured aim point.

Figure 3b shows the definition of terms for an experiment without defined reference positions. Only the *reference distance* between aim points in two consecutive measurements (measurement 1 and measurement 2) is known up to an *uncertainty* of  $\Delta u = \sqrt{2} \cdot u$ . The *measured distance* is defined as the distance between the two consecutively measured focal spot positions. The difference between the reference distance and the measured distance is called the *deviation* in this case.

Figure 3c and d refer to the principle of measurement. In Fig. 3c, the focal spot is sketched. With a defined frequency, the aim point is shifted by an amplitude, thus performing a periodic movement. A camera captures a sequence of that movement, from which an *amplitude image* is derived, as sketched in Fig. 3d. The amplitude image typically shows two regions of high amplitudes, denoted by *Vertex A* and *Vertex B*. The centers of mass of these vertices are derived with a clustering algorithm. The midpoint between the two centers of mass is denoted the *measured aim point*.

Since there is no absolute reference in the system of Themis, the measured offsets between two consecutive measurements are used for differential evaluation, i.e. two consecutive measurements are taken, before and after a defined displacement of the spot for comparison of distance. With the position of the heliostats in the field and the number of increments (drive rotation/encoder resolution:  $\Delta\alpha_i=0.13$  mrad/inc) of the drive performing the shift, the expected offset can be calculated. However, this holds an uncertainty. At least  $\pm 1$  increment must be considered for the respective drive for one position. In this work an uncertainty in mm at the target according to

$$u = \pm\sqrt{2(2\Delta\alpha_i n_i D_s)^2} \quad 1)$$

is used for the reference of the aim point position. It includes the slant range  $D_s$  between the heliostat and the respective aim point, twice the encoder resolution  $\Delta\alpha_i$  and the number of increments  $n_i$  ( $=1$ ) to take the reflection into account. Backlash is neglected with this simplified approach.

For heliostat B12 (refer to Fig. 2 for position of heliostat ID) with a slant range of 89 m towards the flux target plane, this results in an estimated minimal uncertainty of  $\pm 23$  mm for each axis and a total estimated pointing precision of 33 mm, assuming a newly calibrated heliostat and relative positioning only. Heliostat E07 is assumed to have an uncertainty of 45 mm at the same target. At the cavity, the uncertainty for B10 is 36 mm. For the measurement of aim point distances, the combined uncertainty is  $\Delta u=51$  mm, following standard uncertainty propagation. The image sequences were taken with a PCO.edge 4.2 camera at a reduced resolution of 512x512 pixels, which results in a spatial resolution of the receiver and target areas of about 20 mm/pixel.

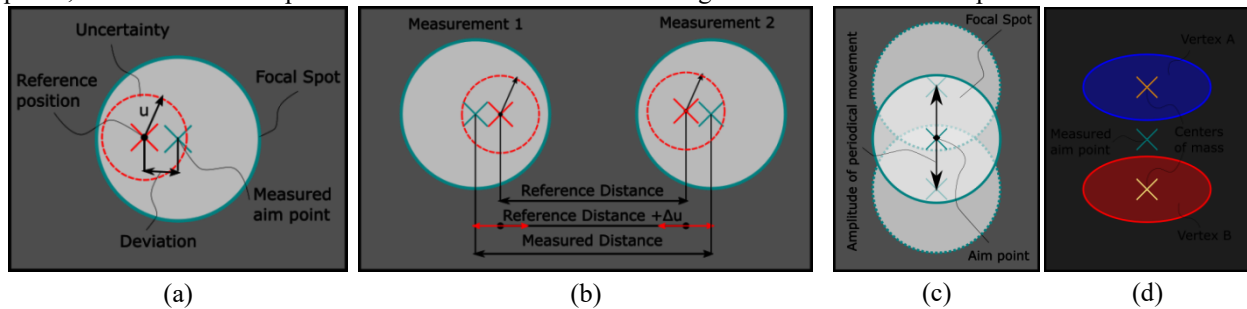


Figure 3: Definition of measurement terms. (a) Measurement of a single spot: the *reference position* is the position where the spot is expected to be. The *uncertainty* of the reference position is marked as a radius around the reference position coordinate. The *measured aim point* has a *deviation* from the reference position. (b) Measurement of distance between two spots: Two reference positions have an expected *reference distance* with an *uncertainty* of  $\Delta u$ . The measured distance, derived from two aim point measurements of focal spots has a different distance than the reference distance, denoted by *deviation of distance*. (c) Sketch of the periodic movement of the focal spot. The movement is carried out with a defined frequency and amplitude of movement around the true aim point. The evaluation of a image sequence of this movement results in the amplitude image. (d) Amplitude image revealing two regions of high amplitudes, denoted as vertices (red and blue region). The mean of the center of mass of both vertices (yellow and orange cross) is regarded the measured aim point (green cross).

## Measurement at Large Flux Target

The heliostats B12 and E07 were pointed aside of each other to the large target, moving periodically with 0.23 Hz horizontally (B12) and with 0.16 Hz vertically (E07). The setup allows for the retrieval of the aim position of each heliostat. For the individual spot, the representative position was retrieved similarly to the state-of-the-art calibration procedure as described by Berenguel et al.<sup>1</sup> from the captures, resulting in the coordinates  $X, Z=(-1.469 \text{ m}, -17.025 \text{ m})$  for B12 and  $X, Z=(1.585 \text{ m}, -16.667 \text{ m})$  for E07, given in the local target coordinate system.

The result of the simultaneous evaluation of the image sequence according to the HelioControl-method is displayed in Fig. 4 right, showing the retrieved contours from the vertices of movement, the target borders and the resulting representative position of the two focal spots. The identified positions are  $X, Z=(-1.462 \text{ m}, -17.036 \text{ m})$  for B12 and  $X, Z=(1.594 \text{ m}, -16.671 \text{ m})$  for E07 respectively. The distances to the reference positions of the foci is 13 mm and 10 mm respectively, which is below the resolution of the experiment of  $\sim 20 \text{ mm/pixel}$  and far below the estimated uncertainty of pointing of the heliostats.

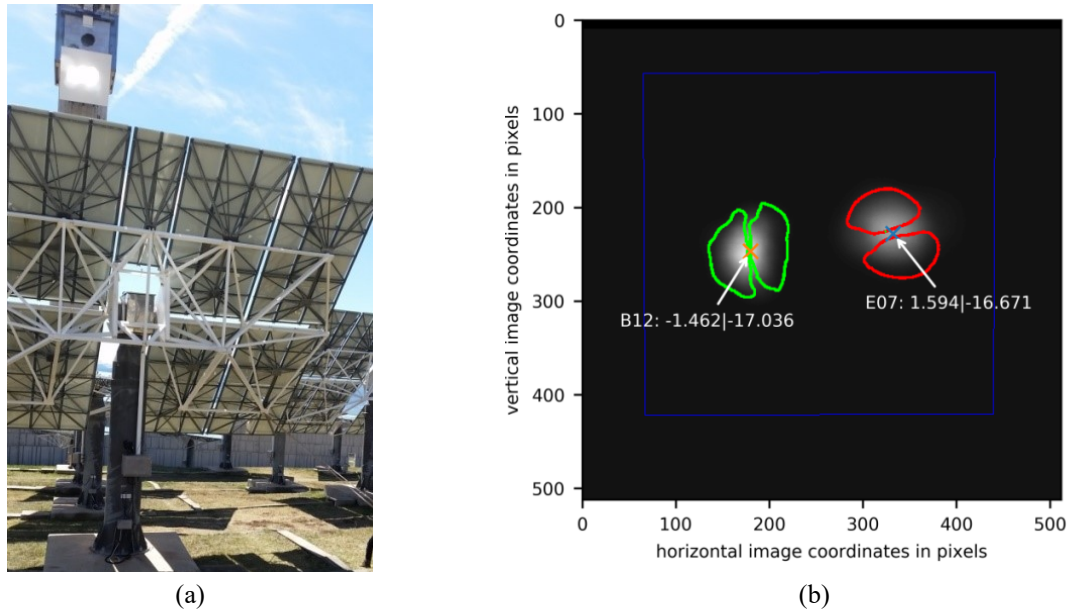


Figure 4: a) View from the heliostat field to the target underneath the cavity receiver during an experiment. b): First frame of the captured sequence with the contours of the retrieved vertices (green and red) of each movement and the resulting coordinate of the identified aim point for the heliostats B12 and E07. The blue rectangle shows the target borders in the camera's field of view.

## Measurement at the Small Cavity Receiver

Experiments conducted at white flux targets allow for simple referencing of the representative aim points, however, they restrict the number of heliostats overlapping due to temperature constraints. The experimental setup at the small cavity receiver “Mini Pegase” of the Themis system allowed for a larger part (up to 16 heliostats) of the field to be on target. The receiver was equipped with a water cooled panel at the back in order to avoid overheating.

Images of the receiver and the experimental setup are given in Fig. 5. Figure 5a), the small cavity with an aperture of 1.2 m x 1.2 m and a depth of about 0.8 m is shown. Its position at the tower is indicated in Fig. 5c). Figure 5b) and 5d) show images during an experiment with the receiver under concentration. The protective steel plates around the cavity, insulation material, the steel cavity walls and the aluminum panel at its back each have very different reflectivity. The steel and aluminum components have a high share of specular reflectivity. Together with the diverse surface angles in the field of view, local peaks and minima are visible in the measurement signal.

To compensate for the locally diverse reflectivity, a simplified relative reflectance map has been calculated. Experiments with single heliostats aiming at the receiver area and performing a periodic movement have been used for the generation of this map after the measurement campaign. These experiments were not conducted for that purpose and hence only allow for the generation of a map with reduced extent of validity and confidence.

For highly variable surface properties and regions with specular reflectance at different local incident angles, receiver reflectance correction models specific for each heliostat are needed. With the data base captured at the measurement campaign, only a model for a restricted range of incidence angles could be generated. Therefore, experiments with the heliostats B10 and B04 (referring to Fig. 2) were used, disregarding the small deviation of incidence angle of a few degrees. The effect of the correction is displayed in Fig. 6.

The evaluation of two conducted experiments I and II, each of them comprising two measurements, is presented here. The assessment of the derived locations of aim points among the cumulative flux is performed as comparison between two consecutive aim point measurements. Between the single measurement in the experiment, the aim point is displaced with a certain amount of the drive increments of the heliostats. Lacking an absolute aim point measuring reference system at Themis, the positional differences between a first and a second measurement are evaluated (refer to Fig. 3b). This is a simplification for a first assessment on a receiver of that kind.

The first experiment I involved a total of 9 heliostats pointing at the Mini-Pegase cavity receiver, four of them moving at different frequencies, five pointing statically. Here, we concentrate on the evaluation of the signal of heliostat B10 with a frequency of movement of 0.1 Hz around the elevation axis. During a first measurement it was aimed at the center of the cavity receiver. In a second measurement it was shifted by 10 increments to the right (west) resulting in an estimated displacement of  $320 \text{ mm} \pm 51 \text{ mm}$ .

The second experiment II is a repetition of the first one, but with further static heliostats added. Besides the four moving heliostats (marked in red in Fig. 2), 12 static heliostats (marked in green in Fig. 2) were contributing to the total flux.

The four image sequences taken at the two experiments were evaluated for their amplitude and phase information at the frequency of movement of heliostat B10 of 0.1 Hz. Exemplarily the amplitude image of B10 in the first measurement of experiment I is shown in Fig. 6a. The signal is clearly extracted from the cumulative flux, showing two regions (vertices) of high amplitude, i.e. of high variance of intensity of the image sequence. These regions show the effect of the slope of the focal spot moving up- and downwards in the periodical pattern. However, the high reflectivity of the back panel and the low reflectance of the surrounding sheets with respect to the angle of view hide a share of the signal. Fig. 6b shows the same amplitude image with the simplified receiver correction model applied. The correction reveals the actual extent of the signal provided by the heliostat movement.

The full evaluation of the experiments was conducted using the corrected amplitude and reflection invariant phase information to extract the relevant share from the cumulative flux and to feed a clustering algorithm. The algorithm follows the methodology as described in earlier publications<sup>9</sup>, extended by the named phase information. The algorithm derives exactly two clusters and cluster centers in image coordinates depending on the amplitude and the phase. The results of the discrimination and clustering algorithm is displayed in Fig. 7 and listed in Tab. 1. Images (a) and (b) show the results of the two measurements from experiment I, (c) and (d) belong to experiment II respectively.

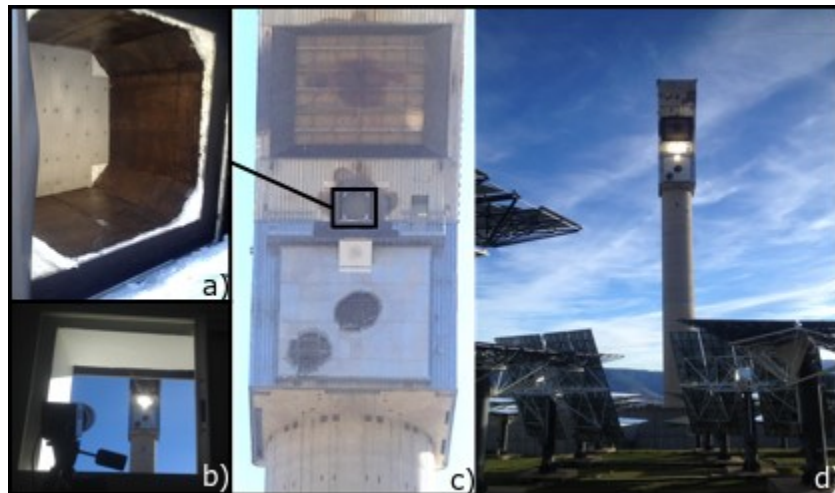


Figure 5: Images of the small cavity receiver “Mini-Pegase” and the measurement setup. a) Close up of the cavity aperture, also visible in c). b) view from the control room showing the camera used and the receiver during an experiment. c) Image of the receiver area with the small cavity marked d) View from the heliostat field at the Themis tower during an experiment.

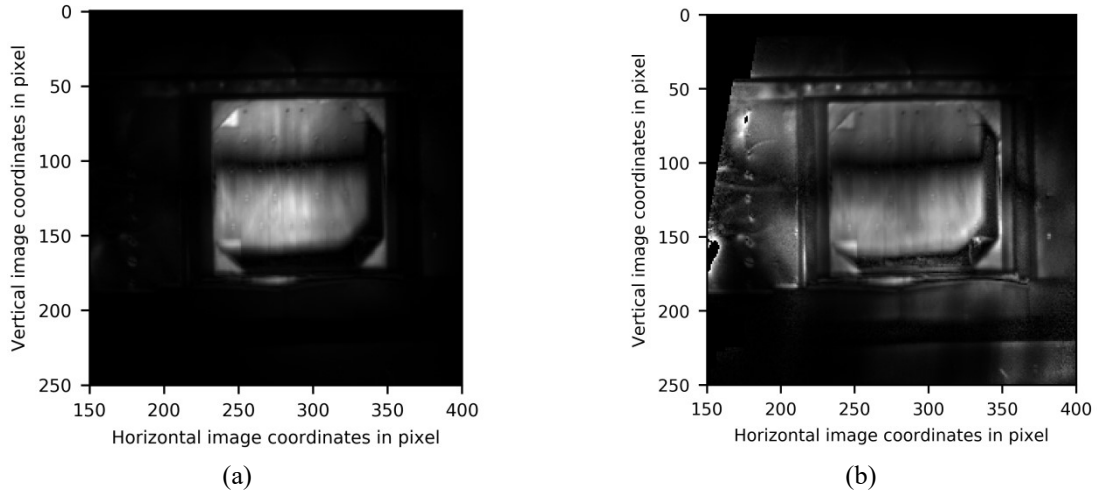


Figure 6: (a) Preliminary amplitude image of heliostat B10 at 0.1Hz at the cavity receiver, extracted from the cumulative flux of 9 heliostats on target. The two bright regions mark the distributions of highest amplitude, i.e. the vertices of the regions with the highest slope in the flux distribution of the respective heliostat spot. The high variance of reflectivity hides a share of the spot. In the image, only the projection on the highly reflective back panel is visible. (b) Correction of the amplitude image displayed in (a). The application of the simple receiver model shows the extent of the signal after correction. Nevertheless, local peaks and gaps in the distribution originate from the simplifications, leaving room for an improved receiver reflectance model

The blue and red regions denote the regions covered by the two vertices from the amplitude image, classified into two clusters by use of the k-means-algorithm involving amplitude and phase. The cluster centers are marked as orange and yellow crosses in the images. The representative aim point is in the center of the two clusters, marked by the green cross. The points derived in image coordinates are transferred to the coordinate system of the Themis plant for comparison and the distance between the first and second aim point measurement in each experiment was derived. In experiment I, a focal spot distance of 340 mm between the two measurements was found, i.e. showing a deviation of 20 mm towards the expected reference distance. Experiment II showed a distance between the two focal spots of 357 mm, exceeding the reference distance by 37 mm. Both measured distances are within the uncertainty of the reference distance of  $\Delta u=51$  mm for the differential positioning. For a thorough statistical evaluation of measurement uncertainty, however, a larger number of experiments is recommended to be conducted in future.

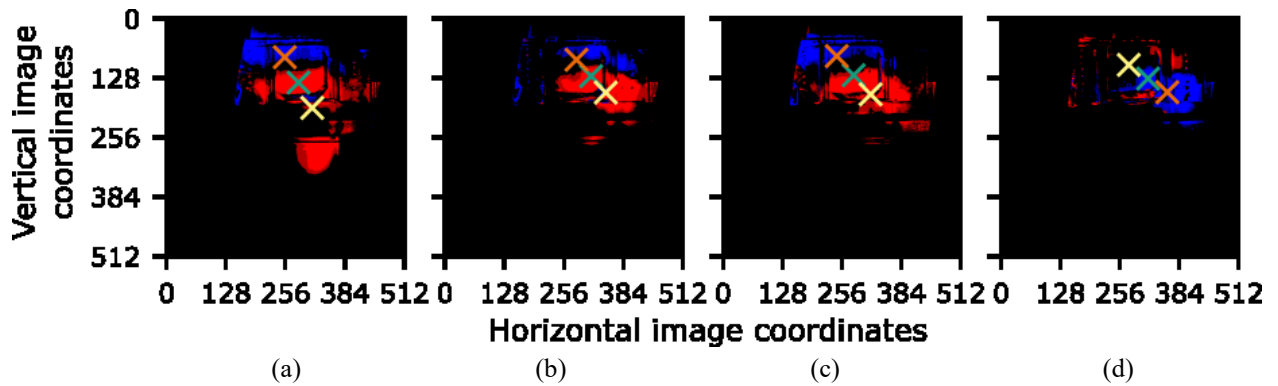


Figure 7: Classified amplitude images of experiment I ((a) and (b)) and II ((c) and (d)). The red and blue color mark the classification of each pixel in the amplitude image to one of two centers by the k-means clustering algorithm, based on amplitude and phase information. The color intensity reflects the amplitude of movement after correction with the simplified receiver reflectance correction model. The orange and yellow cross mark the cluster centers with its mean (green cross) indicating the found representative aim point.

**TABLE 1.** Results of the experiments conducted in the measurement campaign. The results of the measurement with heliostats B12 and E07 at the flux target are given with respect to a reference aim point measurement as absolute values. The results of the experiments at the cavity with heliostat B10 are given as deviations between the calculated expected reference distance of two aim point positions and the derived distance between the two aim point positions measured within one experiment. The uncertainty of the calculated heliostat pointing position and reference aim point distance is given as combined uncertainty for the two positions.

<b>Heliostat Name</b>	<b>Target</b>	<b>Slant range in m</b>	<b>Deviation in mm</b>	<b>Deviation in mrad</b>	<b>Combined uncertainty in mm</b>
B12	Flux Target	90	13	0.11	33
E07	Flux Target	122	10	0.08	45
B10	Cavity Receiver	98	20	0.20	51
B10	Cavity Receiver	98	37	0.38	51

## CONCLUSION

The measurement campaign on the HelioControl-method, conducted at the Themis central receiver facility gave valuable experiences and promising experimental results, both with respect to proof of concept and expected range of uncertainty in measurement.

For the first time, the HelioControl system, implemented as a basic prototype of the envisioned plugin could be integrated into the control structure of an experimental heliostat field. The implementation of the communication link between Hyperviseur and HelioControl, as well as the modification of the heliostats to perform periodic movements with defined frequencies, was implemented within a few days. This reveals the small required effort for implementing such a plugin into an existing field control. Especially in modern control networks, where updates can be distributed remotely, a heliostat field could be adapted quickly.

The experiments conducted with the homogeneous flux target show, compared to the expected position, aim point measurement deviations of the methodology in the low centimeter range, being below the estimated uncertainty of the tracking mechanism. After the extraction of the heliostat signal, image processing algorithms with reasonable computational cost must be applied for evaluation to obtain representative and more than satisfactory results. The restriction of the target for higher incident flux did not allow for the measurements with many overlapping heliostats, however, the experiments show the capability of the method. In simulations, the algorithm demonstrated its capability to identify aim points from 9000 overlapping spots.

The experiments at the Mini-Pegase cavity receiver were more challenging due to the variable reflectivity in the field of view of the camera. However, with the application of a simple reflectance correction model derived from experiments, sufficing evaluation signals could be retrieved from the measurements. In the tests, the deviations between the measurement and the reference values were below the uncertainty of the latter.

For a representative evaluation of the uncertainty to expect and practicability in plant operation further comprehensive assessments and full statistical evaluation are needed. The first results obtained in the campaign, however, support the feasibility of the concept. For commercial receivers with far more homogeneous receiver surfaces with respect to reflectivity, satisfying uncertainties can be expected with small effort. Future experiments with high numbers of heliostats are the next essential step for the proof of feasibility of the HelioControl method.

## ACKNOWLEDGMENTS

This work has been supported by the German Federal Ministry for Economic Affairs and Energy (BMWi) under contract 0324175 and by the French “Investments for the future” program managed by the National Agency for Research, under contract ANR-10-EQPX-49-SOCRATE (Equipex SOCRATE). Financial support of the SFERA II project – Transnational Access activities (EU 7th Framework Programme Grant Agreement n° 312643) is gratefully acknowledged.

## REFERENCES

1. M. Berenguel, F. R. Rubio, A. Valverde, P. J. Lara, M. R. Arahall, E. F. Camacho, and M. Lopez, "An artificial vision-based control system for automatic heliostat positioning offset correction in a central receiver solar power plant," *Solar Energy* **76** (5), 563–575 (2004).
2. C. Iriarte-Cornejo, C. A. Arancibia-Bulnes, J. Waissman, R. E. Cabanillas, and C.A. Estrada, "Dynamic Drift Compensation for Heliostats," *Energy Procedia* **49**, 2109–2117 (2014).
3. M. Escobar-Toledo, C. A. Arancibia-Bulnes, C. Iriarte-Cornejo, J. Waissman, D. Riveros-Rosas, R. E. Cabanillas, and C. A. Estrada, "Heliostat image drift behavior for different error sources," *Journal of Renewable and Sustainable Energy* **6** (2), 23117 (2014).
4. A. Kribus, I. Vishnevetsky, A. Yogev, and T. Rubinov, "Closed loop control of heliostats," *Energy* **29** (5-6), 905–913 (2004).
5. M. R. Convery, "Closed-loop control for power tower heliostats," in *SPIE Solar Energy + Technology*, edited by K. VanSant and R. A. Sherif (SPIE, 2011), 81080M-81080M-8.
6. P. J. Harper, J. Dreijer, K. Malan, J. Larmuth, and P. Gauche, "Use of MEMs and optical sensors for closed loop heliostat control," in *AIP Conference Proceedings 1734* (AIP Publishing, Melville, New York, 2016), p. 70015.
7. N. Goldberg, G. Kroyzer, R. Hayut, J. Schwarzbach, A. Eitan, and S. Pekarsky, "Embedding a Visual Range Camera in a Solar Receiver," *Energy Procedia* **69**, 1877–1884 (2015).
8. G. Bern, P. Schöttl, A. Heimsath, and P. Nitz, "Novel Imaging Closed Loop Control Strategy for Heliostats," *AIP Conference Proceedings* **2017** (1850), 030005.1 - 030005.10 (2017).
9. G. Bern, P. Schöttl, D. W. van Rooyen, A. Heimsath, and P. Nitz, "Parallel in-situ measurement of heliostat aim points in central receiver systems by image processing methods," *Solar Energy* **180**, 648–663 (2019).